

Localization deception performance of FDA signals under passive bi-satellite reconnaissance

Haoliang GUAN¹, Shunsheng ZHANG^{1*} & Wen-Qin WANG²

¹Research Institute of Electronic Science and Technology, University of Electronic Science and Technology of China, Chengdu 611731, China;

²School of Information and Communication Engineering, University of Electronic Science and Technology of China, Chengdu 611731, China

Received 22 October 2019/Revised 6 December 2019/Accepted 20 January 2020/Published online 18 August 2021

Abstract Time difference of arrival (TDOA) and frequency difference of arrival (FDOA) are widely adopted for passive bi-satellite positioning system (BPS) localization. Although TDOA/FDOA localization countermeasures have received much attention, different from existing passive localization countermeasure techniques which mainly concentrate on designing spoofing jammers. This paper proposes that the application of frequency diverse array (FDA) antenna has more advantages in achieving localization deception compared with phased array (PA) antenna. FDA uses a small frequency offset across its array elements, which makes periodical time-variance beampattern even at a fixed angle and distance. Followed by this new method, closed-form expressions for the geometric dilution of precision (GDOP) and Cramer-Rao bounds (CRB) are derived to quantitatively evaluate the localization deception performance of the FDA transmitted signals. Both numerical analysis and simulation results show that FDA indeed provides robust localization deception performance than conventional phased-array under passive bi-satellite reconnaissance.

Keywords localization deception, passive bi-satellite reconnaissance, frequency diverse array (FDA), Cramer-Rao bound (CRB), time difference of arrival (TDOA), frequency difference of arrival (FDOA)

Citation Guan H L, Zhang S S, Wang W-Q. Localization deception performance of FDA signals under passive bi-satellite reconnaissance. *Sci China Inf Sci*, 2021, 64(9): 192305, <https://doi.org/10.1007/s11432-019-2773-1>

1 Introduction

Compared with active localization, passive localization does not emit electromagnetic waves and passively estimates the location of the emitter. It has attracted more and more attention due to the advantages of strong concealment, good flexibility, and high precision [1, 2]. Typical interception techniques in passive localization include the received signal strength (RSS) [3], time-of-arrival (TOA) [4, 5] and angle-of-arrival (AOA) [6], but time difference of arrival (TDOA) and frequency difference of arrival (FDOA) are more popular for passive bi-satellite positioning system (BPS) [7, 8]. Although many methods have been proposed against active localization reconnaissance techniques, few effective passive localization techniques are available due to the high concealment of passive localization technology. False multi-target formulation and radio frequency (RF) stealth are two main countermeasure methods for passive localization. The former requires the participation of a spoofing jammer for distributed false targets or dense false targets [9–11], but its performance may be degraded by the jamming signals. The latter is to reduce the probability of interception for passive localization technique by proper waveform design and transmit beamforming [12, 13], but the designed waveforms are usually difficult to implement in practice.

In this paper, we propose a passive localization deception scheme using frequency diverse array (FDA) antenna because FDA provides potential localization deception capability. Localization deception was firstly applied against global position systems (GPS) [14]. We analyze the passive localization deception performance of FDA signals under passive BPS using TDOA/FDOA which includes two stages. In the first stage, the TDOA/FDOA is estimated from the signals received by the two satellites with the cross

* Corresponding author (email: zhangss@uestc.edu.cn)

ambiguity function (CAF) [15–17]. In the second stage, the TDOA and FDOA localization equations are solved with the estimation information in the first stage [18, 19]. Note that, this considers mainly localization deception in the first stage.

FDA concept was firstly introduced by the Air Force Research Laboratory [20–22]. Unlike conventional phased array (PA) radar that has the same carrier frequency in all array elements, FDA uses a small frequency increment across its array elements to generate a transmit beampattern as a function of angle, range and time [21–24]. Moreover, an S-shaped coupling beampattern will be produced for a standard FDA using linearly progressive frequency increments (ULA FDA) [25]. Several non-standard FDA structures using nonlinearly increasing frequency offsets, such as time-dependent [26, 27], random frequency increments [28], central symmetrical [29, 30], and logarithmic [31], have been proposed to decouple FDA range-angle beampattern. More importantly, even for a fixed angle and/or range, FDA still produces a time-variant beampattern. As a consequence, the signal-to-noise ratio (SNR) will be reduced, leading to lower estimation accuracy.

In this paper, we make a rigorous theoretical analysis of the localization deception performance of FDA transmitted signals under passive bi-satellite reconnaissance, together with simulation verifications. Our main contributions are listed as follows:

(i) We provide a rigorous theoretical analysis of the localization deception performance of FDA transmitted signals under TDOA and FDOA joint passive bi-satellite reconnaissance. Closed-form expressions are derived for the geometric dilution of precision (GDOP), which represents an intuitive positioning accuracy of the reconnaissance.

(ii) The Cramer-Rao bounds (CRBs) of the passive bi-satellite reconnaissance in estimating the parameters of the FDA signals are derived, along with numerical analysis.

The rest of this paper is organized as follows. In Section 2, we specifically analyzed the time-varying characteristics of the FDA beampattern. Then, the CAF-based joint TDOA and FDOA estimation of FDA transmitted signals under passive bi-satellite reconnaissance is present. In Section 3, the CRB and GDOP of FDA transmitted signals under passive bi-satellite reconnaissance are derived. Next, numerous examples are provided in Section 4. Finally, conclusions are drawn in Section 5.

2 Geolocation reconnaissance of FDA signals

Consider an M -element FDA emitter with the frequency offset Δf_m and the following radiation frequency for the m th element:

$$f_m = f_0 + \Delta f_m, \quad m = 1, 2, \dots, M - 1, \quad (1)$$

where f_0 denotes the reference carrier frequency. When a monochromatic waveform is adopted and the m th element transmitted signal is $s_m(t) = \phi(t) \exp(-j2\pi f_m t)$, where $\phi(t)$ is the transmitted baseband complex waveform with unit energy, namely, $\int_T \phi(t) \phi^H(t) = 1$, where T and $(\cdot)^H$ are the pulse duration and conjugate operator, respectively. The whole transmitted signals can then be written as

$$s(\theta, r, t) = \sum_{m=0}^{M-1} \frac{1}{r_m} \phi(t) \exp \left\{ -j2\pi f_m \left(t - \frac{r_m}{c} \right) \right\}, \quad (2)$$

where $r_m \approx r - md \sin \theta$ denotes the slant range for the far-field fixed reconnaissance point (θ, r) , θ being the azimuth angle and r the range for the first element, $\phi_0 = -2\pi f_0(t - \frac{r}{c})$, c is the speed of light. Since $r_m \approx r - md \sin(\theta)$, Eq. (2) can be rewritten as

$$s(\theta, r, t) \approx \frac{1}{r} \exp(j\phi_0) \sum_{m=0}^{M-1} \exp \left\{ -j2\pi \left[\Delta f_m \left(t - \frac{r}{c} \right) - \frac{f_0 m d \sin \theta}{c} - \frac{m \Delta f_m d \sin \theta}{c} \right] \right\}. \quad (3)$$

Therefore, FDA transmitted beampattern will vary with time, angle, and even range. This implies that FDA transmitted signals will add constructively in certain regions, while destructively in others, providing a possibility of localization deception. More investigations will be provided in the subsequent sections. Note that for ULA FDA, the radiation frequency for the m th element is

$$f_m = f_0 + (m - 1) \Delta f, \quad m = 1, 2, \dots, M - 1. \quad (4)$$

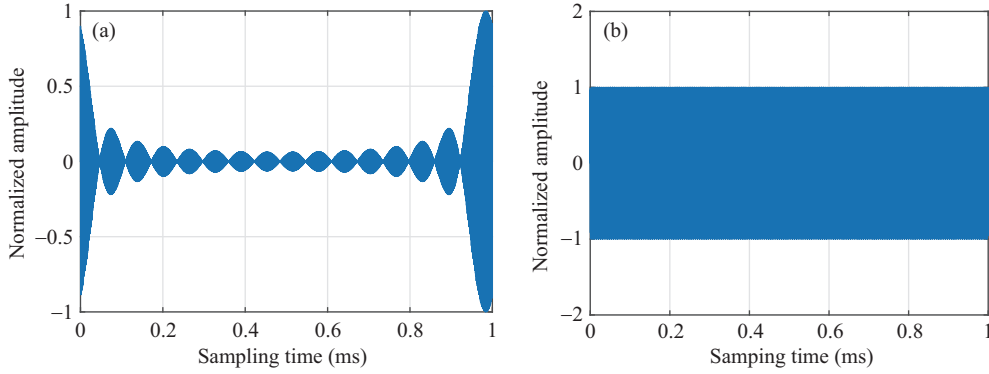


Figure 1 (Color online) Received signal model by BPS. (a) FDA; (b) PA.

Then the amplitude of ULA FDA transmitted signal in far-field is expressed as

$$|s(\theta, r, t)| = \left| \frac{\sin(M\varphi)}{\sin(\varphi)} \right|, \quad \varphi = \Delta f \left(t - \frac{r}{c} \right) - \frac{f_0 \sin \theta}{c}, \quad (5)$$

where $|\cdot|$ is determinant operator. Eq. (5) arrives at the maximum when $\varphi = kn$, where n being an integer. Solving for t yields,

$$t = \left(\frac{1}{\Delta f} \right) k + \frac{r}{c} - \frac{f_0 d \sin \theta}{\Delta f c}. \quad (6)$$

This means its time periodicity is $1/\Delta f$. Figure 1(a) and (b) respectively shows the received ULA FDA and PA signal by BPS. Unlike the traditional PA whose amplitude is the same during the sampling period, the amplitude of the FDA signal varies with the sampling time.

Without loss of generality, we assume a flat earth model and the emitter is located at the earth plane, as shown in Figure 2. The signal received by the i th reconnaissance satellite at fixed angle θ and distance r can be written as (7), where τ_i and ξ_i denote the time delay and Doppler shift between two receivers, respectively. Note that $w_i(t)$ denotes uncorrelated Gaussian noise. The discrete samples $\Upsilon_i(\theta, r, nT_s)$ of (7) is given in (8), where T_s is the sampling period and N is the number of received signal samples.

$$\begin{aligned} \Upsilon_i(\theta_i, r_i, t) &\approx \frac{1}{r_i} \exp[j\xi_i t - j2\pi f_0(t - \tau_i)] \\ &\times \sum_{m=0}^{M-1} \exp \left\{ -j2\pi \left[\Delta f_m(t - \tau_i) - \frac{f_0 m d \sin \theta_i}{c} - \frac{m \Delta f_m d \sin \theta_i}{c} \right] \right\} + w_i(t), \quad i = 1, 2, \end{aligned} \quad (7)$$

$$\begin{aligned} \Upsilon_i(\theta_i, r_i, nT_s) &\approx \frac{1}{r_i} \exp[j\xi_i nT_s - j2\pi f_0(nT_s - \tau_i)] \\ &\sum_{m=0}^{M-1} \exp \left\{ -j2\pi \left[\Delta f_m(nT_s - \tau_i) - \frac{f_0 m d \sin \theta_i}{c} - \frac{m \Delta f_m d \sin \theta_i}{c} \right] \right\} \\ &+ w_i(nT_s), \quad i = 1, 2. \end{aligned} \quad (8)$$

Denoting the TDOA $\tau = \tau_2 - \tau_1$ and FDOA $f = \xi_2 - \xi_1$, according to the CAF principle [8], we can get

$$A(g\Delta\tau, f) = \frac{1}{N} \sum_{n=0}^{N-1} \Upsilon_1^*[nT_s] \Upsilon_2[nT_s + g\Delta\tau] \exp[-j2\pi f nT_s], \quad (9)$$

where ‘*’ denotes the complex conjugation, g is the discrete time delay index and $\Delta\tau$ is the time delay resolution, which means the TDOA parameter $\tau = g\Delta\tau$. In this case, Eq. (9) can be reformulated as

$$A(\tau, f) = \frac{1}{N} \sum_{n=0}^{N-1} \Upsilon_1^*[nT_s] \Upsilon_2[nT_s + \tau] \exp[-j2\pi f nT_s]. \quad (10)$$

Taking fast Fourier transform (FFT) by each time delay, we can find the CAF $A(\tau, f)$. Specifically, the TDOA and FDOA are estimated simultaneously by searching the peaks of $A(\tau, f)$. In doing so, the

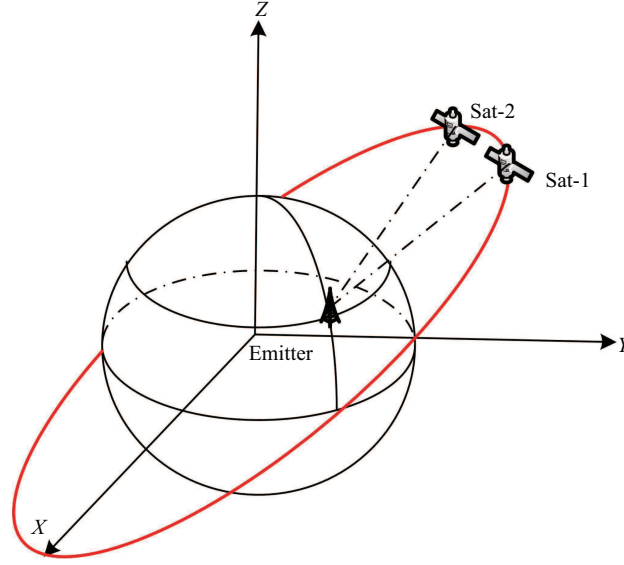


Figure 2 (Color online) Sketch map of BPS localization scenario.

emitter can be localized by solving the following equations:

$$\tau = \frac{1}{c} (\|\mathbf{p}_1 - \mathbf{q}\|_2 - \|\mathbf{p}_2 - \mathbf{q}\|_2), \quad (11)$$

$$f = \frac{f_0}{c} \left[\frac{\mathbf{v}_2 (\mathbf{p}_2 - \mathbf{q})}{\|\mathbf{p}_2 - \mathbf{q}\|_2} - \frac{\mathbf{v}_1 (\mathbf{p}_1 - \mathbf{q})}{\|\mathbf{p}_1 - \mathbf{q}\|_2} \right], \quad (12)$$

$$\frac{x^2}{a_e^2} + \frac{y^2}{a_e^2} + \frac{z^2}{b_e^2} = 1, \quad (13)$$

where f and τ represent the FDOA and TDOA parameters, $\mathbf{q} = [x, y, z]^T$ is the emitter's position vector in earth-centered earth-fixed coordinate system (EFCS) and $a_e = 6378.245$ km, $b_e = 6356.755$ km. Note that the flight paths of the two reconnaissance satellites are denoted by $\mathbf{p}_i = [x_i, y_i, z_i]^T$ and $\mathbf{v}_i = [v_{xi} \ v_{yi} \ v_{zi}]^T$ ($i = 1, 2$), respectively. $\|\cdot\|_2$ represents the two norms of the matrix and $[\cdot]^T$ is the transpose operator.

3 Theoretical reconnaissance bounds of FDA signals

In order to examine the localization deception performance of FDA signals under passive bi-satellite reconnaissance, in this section, the theoretical reconnaissance bounds of CRB are derived and compared with those of conventional PA signals. CRB provides offline estimation accuracy of specific parameters that can be achieved, which is commonly used for analyzing the performance of parameters estimation accuracy. More, we also derived the GDOP, which evaluates the positioning accuracy under FDOA and TDOA measurements and represents an intuitive positioning accuracy of the reconnaissance. Compared with CRB, GDOP can be used to characterize the localization performance under the combined influence of TDOA error, FDOA error, high error and so on. When all the ranging errors are zero-mean independent and identically distributed Gaussian processes with the same variance σ^2 , the relation between CRB and GDOP is shown in

$$\text{GDOP}(\mathbf{q}) = \frac{\sqrt{\text{CRB}(\mathbf{q})}}{\sigma}. \quad (14)$$

3.1 CRB

Reconsidering the received discrete signal (7), we notice that the unknown parameters can be formulated as $\phi = [\tau \ f]^T$, where $\tau = \tau_2 - \tau_1$ and $f = \xi_2 - \xi_1$ are the TDOA and FDOA, respectively. Let's define $\Upsilon = [\Upsilon_1(\theta_i, r_1, nT_s) \ \Upsilon_2(\theta_i, r_2, nT_s)]^T$, $\mathbf{s}_\phi = [s_1(\theta_i, r_1, nT_s) \ s_2(\theta_i, r_2, nT_s)]^T$. Assume that the received

data vector Υ has a Gaussian probability density function (PDF) and $w_i \sim \mathcal{N}(0, \sigma_i^2)$, $i = 1, 2$ which can be expressed as (15) [32], where $(\cdot)^{-1}$ is the inverse operator.

$$p(\Upsilon; \phi) = \frac{1}{\det(\pi\mathbf{C})} \exp \left\{ -(\Upsilon - \mathbf{s}_\phi)^H \mathbf{C}^{-1} (\Upsilon - \mathbf{s}_\phi) \right\}, \quad (15)$$

$$\mathbf{C} = \begin{bmatrix} \sigma_1^2 & 0 \\ 0 & \sigma_2^2 \end{bmatrix}. \quad (16)$$

The Fisher information matrix $\mathbf{I}(\phi)$ is derived as (see Appendix A)

$$\mathbf{I}(\phi) = \begin{bmatrix} I_{11}(\phi) & I_{12}(\phi) \\ I_{21}(\phi) & I_{22}(\phi) \end{bmatrix}. \quad (17)$$

Accordingly, the CRBs for FDOA and TDOA are

$$\begin{aligned} \sigma_f^2 &= I_{22}^{-1}(\phi) = \frac{I_{11}(\phi)}{|\mathbf{I}(\phi)|}, \\ \sigma_T^2 &= I_{11}^{-1}(\phi) = \frac{I_{22}(\phi)}{|\mathbf{I}(\phi)|}. \end{aligned} \quad (18)$$

3.2 GDOP

For flat Earth model, the TDOA, FDOA equation and earth spherical equation are respectively shown in (11)–(13). If the TDOA and FDOA estimation errors are δf and $\delta \tau$, the (small) emitter high error is δh . The satellite site errors are respectively $d\mathbf{P} = [dx_i \ dy_i \ dz_i]^T$, ($i = 1, 2$). Considering that the speed of the formation reconnaissance satellites are similar, the speed error is uniformly expressed as $d\mathbf{v} = [dv_x \ dv_y \ dv_z]^T$, which can be obtained by two-line orbital element (TLE). We can get $\frac{\partial \Delta \tau}{\partial \mathbf{q}}$ by differentiating the TDOA equations at the emitter position $\mathbf{q} = [x, y, z]^T$, where $\Delta \tau$ represents the measured TDOA.

$$\begin{aligned} \delta \tau &= \frac{\partial \Delta \tau}{\partial \mathbf{q}} \\ &= \frac{1}{c} \left(\frac{x - x_2}{\|\mathbf{p}_2 - \mathbf{q}\|_2} - \frac{x - x_1}{\|\mathbf{p}_1 - \mathbf{q}\|_2} \right) dx + \left(\frac{x - x_2}{\|\mathbf{p}_2 - \mathbf{q}\|_2} - \frac{x - x_1}{\|\mathbf{p}_1 - \mathbf{q}\|_2} \right) dy + \left(\frac{x - x_2}{\|\mathbf{p}_2 - \mathbf{q}\|_2} - \frac{x - x_1}{\|\mathbf{p}_1 - \mathbf{q}\|_2} \right) dz. \end{aligned} \quad (19)$$

Rewritten (19) in vector form

$$\delta \tau = \frac{\partial \Delta \tau}{\partial \mathbf{q}} = \sum_s \frac{\partial \Delta \tau}{\partial \mathbf{q}} \Delta \mathbf{q} = \boldsymbol{\alpha} \cdot \begin{bmatrix} dx \\ dy \\ dz \end{bmatrix}, \quad s = x, y, z, \quad (20)$$

where $\boldsymbol{\alpha} = [\alpha_{x2} - \alpha_{x1} \ \alpha_{y2} - \alpha_{y1} \ \alpha_{z2} - \alpha_{z1}]$, $\alpha_{sj} = \frac{s - s_j}{c \|\mathbf{p}_j - \mathbf{q}\|_2}$, $j = 1, 2$; $s = x, y, z$.

In a similar way, we can get $\frac{\partial \Delta f_{21}(\mathbf{q})}{\partial \mathbf{q}}$ by differentiating the FDOA equations at the emitter position $\mathbf{q} = [x, y, z]^T$, where $\Delta f_{21}(\mathbf{q})$ is the measured FDOA.

$$\delta f = \frac{\partial \Delta f_{21}(\mathbf{q})}{\partial \mathbf{q}} = \sum_s \frac{\partial f_{21}(\mathbf{q})}{\partial s} ds = \sum_s \left\{ \begin{bmatrix} \frac{-v_{s2}}{\|\mathbf{p}_2 - \mathbf{q}\|_2} + \frac{v_{s2}(s_2 - s)^2}{\|\mathbf{p}_2 - \mathbf{q}\|_2^3} \\ - \left[\frac{-v_{s1}}{\|\mathbf{p}_2 - \mathbf{q}\|_2} + \frac{v_{s1}(s_1 - s)^2}{\|\mathbf{p}_1 - \mathbf{q}\|_2^3} \right] \end{bmatrix} \right\} ds, \quad s = x, y, z. \quad (21)$$

Rewritten (21) in vector form

$$\delta f = \frac{\partial \Delta f_{21}(\mathbf{q})}{\partial \mathbf{q}} = \sum_s \frac{\partial f_{21}(\mathbf{q})}{\partial s} ds = \boldsymbol{\beta} \cdot \begin{bmatrix} \Delta x \\ \Delta y \\ \Delta z \end{bmatrix}, \quad s = x, y, z, \quad (22)$$

where

$$\boldsymbol{\beta} = [\beta_{x2} - \beta_{x1} \quad \beta_{y2} - \beta_{y1} \quad \beta_{z2} - \beta_{z1}],$$

$$\beta_{si} = \frac{-v_{si}}{\|\mathbf{p}_i - \mathbf{q}\|_2} + \frac{v_{si}(s_i - s)^2}{\|\mathbf{p}_i - \mathbf{q}\|_2^3}.$$

Considering the earth constraint equation shown in (13), we get

$$x dx + y dy + \frac{z}{1 - e^2} dz = a_e \delta h. \quad (23)$$

From Eqs. (20), (22) and (23), it follows that

$$\mathbf{C} d\mathbf{q} = d\mathbf{z} - \mathbf{F} d\mathbf{p}_1 + \mathbf{K} d\mathbf{p}_2 + \mathbf{H} d\mathbf{v}, \quad (24)$$

where

$$\mathbf{C} = [\boldsymbol{\beta} \quad \boldsymbol{\alpha} \quad \mathbf{q}]^T,$$

$$\mathbf{F} = \begin{bmatrix} \beta_{x1} & \beta_{y1} & \beta_{z1} \\ \alpha_{x1} & \alpha_{y1} & \alpha_{z1} \\ 0 & 0 & 0 \end{bmatrix}, \quad \mathbf{K} = \begin{bmatrix} \beta_{x2} & \beta_{y2} & \beta_{z2} \\ \alpha_{x2} & \alpha_{y2} & \alpha_{z2} \\ 0 & 0 & 0 \end{bmatrix}, \quad (25)$$

$$\mathbf{H} = \begin{bmatrix} \alpha_{x2} - \alpha_{x1} & \alpha_{y2} - \alpha_{y1} & \alpha_{z2} - \alpha_{z1} \\ 0 & 0 & 0 \\ 0 & 0 & 0 \end{bmatrix}, \quad d\mathbf{z} = [\delta f \quad \delta \tau \quad \delta h]^T,$$

$$d\mathbf{v} = [dv_x \quad dv_y \quad dv_z]^T,$$

where \mathbf{C} is the covariance matrix. If the errors are subject to independent zero-mean Gaussian distributions, then the measured error covariance matrix is $\mathbf{R}_z = E[d\mathbf{z} d\mathbf{z}]^T$, the satellite velocity and position covariance matrix is $\mathbf{R}_v = E[d\mathbf{v} d\mathbf{v}]^T$ and the positioning covariance matrix in EFCS is $\boldsymbol{\Gamma} = \mathbf{C}^{-1} \mathbf{Z} (\mathbf{C}^{-1})^T$, where

$$\mathbf{Z} = \mathbf{E} [d\mathbf{q} d\mathbf{q}] + \mathbf{F} d\mathbf{p}_1 \mathbf{F}^T + \mathbf{K} d\mathbf{p}_2 \mathbf{K}^T + \mathbf{H} d\mathbf{v} \mathbf{H}^T. \quad (26)$$

The GDOP of FDA is

$$\text{GDOP}(x, y, z) = \sqrt{\text{tr}(\boldsymbol{\Gamma})}, \quad (27)$$

where $\text{tr}(\cdot)$ denotes the trace of a matrix.

4 Numerical results

To further examine the impact of the FDA signal on the BPS, it must be actually simulated to verify the effectiveness of the proposed approach. This section is divided into two parts. In the first part, we choose a specific example to explore the effect of FDA in localization deception compared with PA under the same conditions. In the second part, we explored the effect of different parameters and types of FDA on the performance of localization deception briefly.

4.1 Performance of FDA Signal in FDOA/TDOA Localization Deception

First, we simulate the localization deception performance of FDA signals in TDOA/FDOA reconnaissance. Consider a 16-element FDA with half-wavelength element spacing, $f_0 = 5$ GHz and $\Delta f = 1$ kHz. In addition, the sampling time is 0.4 s and the input SNR is 5 dB. The other simulation parameters are listed in Tables 1 and 2.

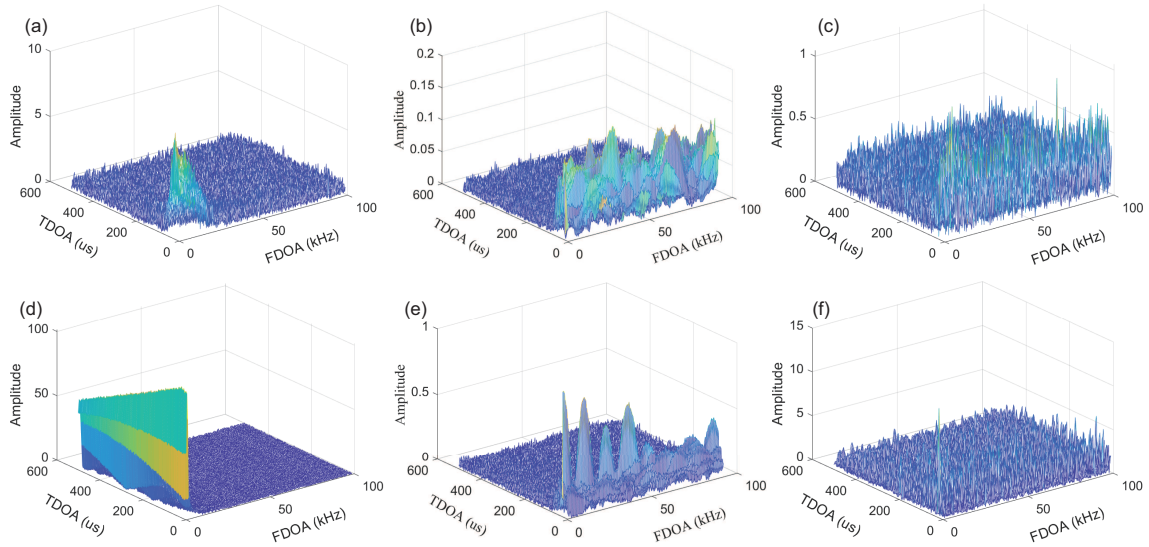
The CAF $A(\tau, f)$ of the received sinusoid FDA and PA signals are shown in Figure 3(a) and (d), respectively. The results demonstrate that the accumulated energy of FDA signals is less than that of PA in the same conditions because of the offset in the FDA signal. It is clear that the CAF of the FDA signal is FDOA multi-peak and has lower energy accumulated. Even if the main peak is found, FDOA and TDOA still cannot be accurately estimated due to lower accumulated energy. Especially in lower SNR

Table 1 Simulation parameters I

Simulation parameters	X	Y	Z
Sat-1 position (km)	3909.0	4499.4	3452.7
Sat-2 position (km)	3892.3	4527.8	3454.5
Sat-1 velocity (km/s)	-1.667	-3.553	6.517
Sat-2 velocity (km/s)	-1.706	-3.510	6.520
Emitter position (km)	3362.1	4006.7	3637.8

Table 2 Simulation parameters II

Simulation parameters	Value
Carrier frequency f_0	1 GHz
Frequency offset Δf	100 Hz
Numbers of elements M	16
Integration time τ_s	10 ms
Intermediate frequency f_b	20 MHz
Sampling frequency f_s	80 MHz
Baseband complex waveform $\phi(t)$	1

**Figure 3** (Color online) Comparison of $A(\tau, f)$ in different transmitted baseband complex waveforms. (a) FDA sinusoid signal; (b) FDA chirp signal; (c) FDA QPSK signal; (d) PA sinusoid signal; (e) PA chirp signal; (f) PA QPSK signal.

environments, its feature will be more noticeable, resulting in better localization deception performance. More investigations provided in the subsequent section also support this conjecture.

In addition, we consider $\phi(t)$ are chirp signal and quadrature phase shift keying (QPSK), respectively. Figure 3 shows the comparison of FDA and PA signals in different transmitted baseband complex waveforms. We can clearly see that the above conclusions also apply to both chirp and QPSK signals, which verified that FDA emitter can provide robust localization deception in radar and communication fields.

Note that except CRB, here, root mean square error (RMSE) is also used as a performance metric, which is shown in

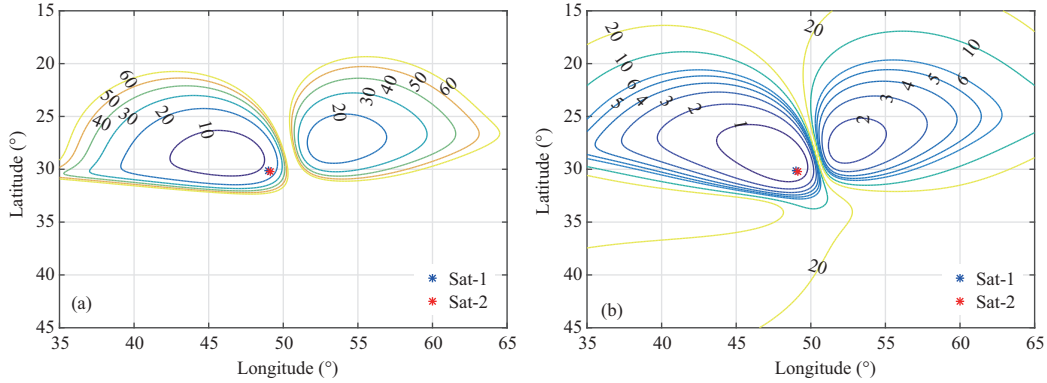
$$Q_\varepsilon = \lim_{N \rightarrow \infty} \frac{1}{N} \sum_{n=1}^N (\varepsilon_n - \hat{\varepsilon}_n) (\varepsilon_n - \hat{\varepsilon}_n)^T, \quad \varepsilon = \tau, v, \quad (28)$$

where N is the number of independent Monte-Carlo simulations, here, $N = 500$. $\hat{\varepsilon}_n$ and ε_n are respectively the n th measured parameter and the real one. τ and f are the TDOA and FDOA, respectively. Q_ε is the RMSE of TDOA or FDOA. In order to clearly show the localization deception performance of FDA, here we define $\Delta Q_\varepsilon, \varepsilon = \tau, f$ shown in

$$\Delta Q_\varepsilon = Q_\varepsilon^{\text{FDA}} - Q_\varepsilon^{\text{PA}}, \quad \varepsilon = \tau, f, \quad (29)$$

Table 3 Comparison of RMSE between FDA and PA parameters estimation

Signal type	SNR (dB)	−10	−5	0	5	10
Sinusoid signal	ΔQ_v (Hz)	279	151	51	43	12
	ΔQ_τ (ns)	21	9	4	≈ 0	≈ 0
Chirp signal	ΔQ_v (Hz)	252	176	87	63	17
	ΔQ_τ (ns)	18	7	2	≈ 0	≈ 0
QPSK signal	ΔQ_v (Hz)	393	152	58	26	3
	ΔQ_τ (ns)	17	4	≈ 0	≈ 0	≈ 0

**Figure 4** (Color online) GDOP comparisons. (a) FDA emitter; (b) PA emitter.

where $Q_\varepsilon^{\text{FDA}}$ and $Q_\varepsilon^{\text{PA}}$ are the RMSE of FDA-related and PA-related parameters, respectively. Table 3 shows the comparison of RMSR between FDA and PA parameters estimation in the same conditions. It is clear that all kinds of FDA signals we consider perform a large FDOA-RMSE error compared with the same PA signals in the low SNR region, which verified the effectiveness of kinds of FDA signals in localization deception applications.

Figure 4 compares the GDOP of PA and FDA under the simulation conditions shown in Tables 1 and 2. The GDOP value decreases with the approaching subastral point, but the ratio between FDA and PA continues to increase. In these conditions, the GDOP ratio value between FDA and PA is less than 4 when the emitter is far from the sub-satellite point. As it approaches the sub-satellite point, this value increases continuously, and it is great than 10 when it approaches the sub-satellite point, which indicates that FDA has better localization deception performance when the emitter is closer to the subastral point.

4.2 Comparison of localization deception performance between FDA and PA under different conditions

Furthermore, we compared the localization deception of FDA and PA under different conditions. As the theoretical analysis shows that time-variance is one of the important reasons for the localization deception of FDA signals, different array parameters are adopted to evaluate their effects on the localization deception performance. The parameters of the reconnaissance satellites are listed in Tables 1 and 2.

Figure 5 shows the influence of the different sampling starting points during the same cycle. The used sampling periods are $\tau_s = k/\Delta f + \zeta/\Delta f$, where k is an integer and ζ is continuous value between 0 and 1. For ULA FDA, its time periodicity is $1/\Delta f$ and the array pattern will scan all angles in $1/\Delta f$. Thus the conclusion followed in this part is not influenced by k when $\tau_s \leq 1/\Delta f$. Figure 5 shows that different time sampling starting point in the same cycle greatly influences the FDOA measurement accuracy. The time variance of FDA signals means that the effective SNR changes with time, angle and distance. This change will sometimes decrease the SNR, leading to lower estimation accuracy. Especially in the strong noise background or weaker received signal conditions, this characteristic becomes more apparent, which also means that FDA exhibits better localization deception in lower SNRs. It should be noted that even in low SNRs, the estimation results of RMSE and CRB are approximate. That is to say, under the given signal processing models, it is reasonable to use CRB to verify the parameter estimation performance of FDA signals.

Figure 6 compares the CRBs of TDOA and FDOA between FDA and PA as a function of the SNR. It is clear that the smaller Δf can achieve a better localization deception effect especially in lower SNRs.

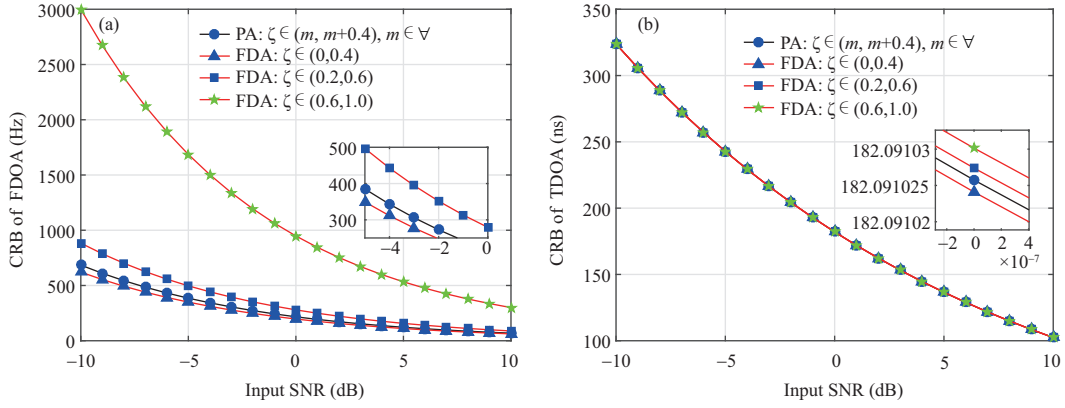


Figure 5 (Color online) CRBs in FDA and PA under different sampling starting points. (a) CRB of FDOA; (b) CRB of TDOA.

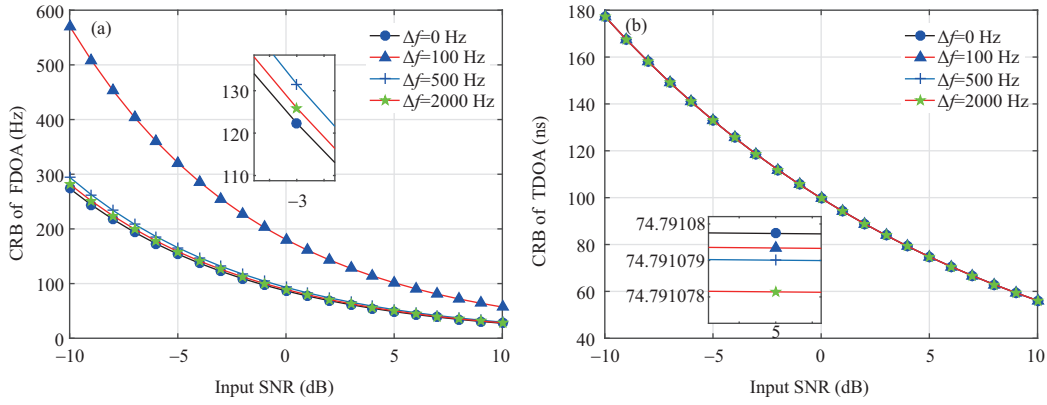


Figure 6 (Color online) CRBs in FDA and PA under different Δf . (a) CRB of FDOA; (b) CRB of TDOA.

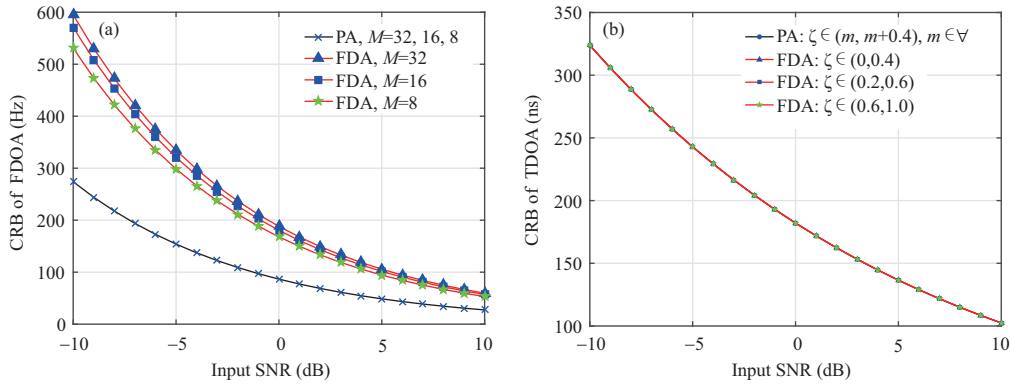


Figure 7 (Color online) CRBs in FDA and PA under different number of elements. (a) CRB of FDOA; (b) CRB of TDOA.

When Δf increases to a certain degree, its localization deception effect will disappear. Therefore, in some radar or communication scenarios where large frequency offsets are applied, its localization deception performance may be poor. In this scenario, other parameters which seriously affect the localization deception performance of the FDA should be optimized as much as possible.

Figure 7 shows the relation between localization accuracy and the number of arrays. We can see that with the increase of array elements, the localization deception performance will also improve. It is noteworthy that the FDA emitter will only pose greater difficulties in the FDOA reconnaissance methods. For TDOA, the FDA seems not to cause too much difficulty theoretically. According to [33], in the BPS scenario, the TDOA equation takes the role of bearing data, and the FDOA signal takes the role of distance measurement. Accurate estimation of FDOA and TDOA is a prerequisite for excellent performance of TDOA/FDOA localization. Therefore, although the TDOA and FDOA cannot be equally affected, FDA

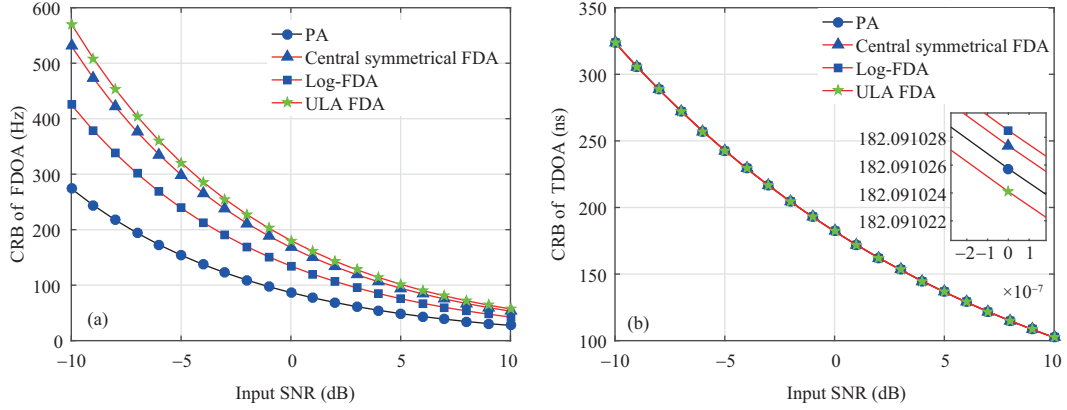


Figure 8 (Color online) CRBs in FDA and PA under different non-standard FDAs. (a) CRB of FDOA; (b) CRB of TDOA.

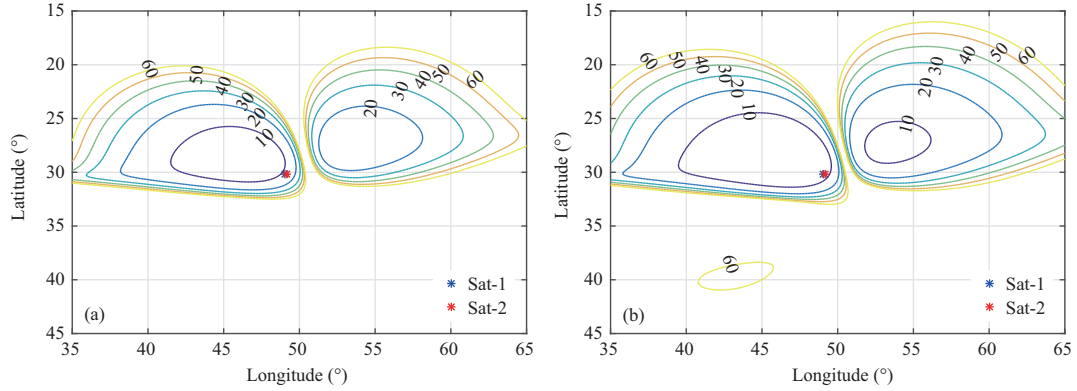


Figure 9 (Color online) GDOP in central symmetrical FDA and log-FDA. (a) Central symmetrical FDA; (b) log-FDA.

Table 4 RMSE comparison under standard and non-standard FDAs

Signal type	SNR (dB)	-10	-5	0	5	10
ULA FDA	ΔQ_v (Hz)	341	176	126	73	53
	ΔQ_τ (ns)	18	4	≈ 0	≈ 0	≈ 0
Log-FDA	ΔQ_v (Hz)	182	121	55	42	36
	ΔQ_τ (ns)	25	9	≈ 0	≈ 0	≈ 0
Central symmetrical FDA	ΔQ_v (Hz)	162	79	70	51	3
	ΔQ_τ (ns)	12	3	≈ 0	≈ 0	≈ 0

can still have great application value in the field of passive localization deception.

In addition, we also considered two non-standard FDAs: central symmetrical FDA and log-FDA. Their frequency offsets are given as follows:

$$\Delta f_{cs} = \begin{cases} \Delta f \left(\frac{M}{2} - \left| m - \frac{M}{2} \right| \right), & m = 0, 1, \dots, \frac{M}{2}, \\ \Delta f \left(\frac{M}{2} - \left| m - \frac{M}{2} \right| - 1 \right), & m = \frac{M}{2}, \frac{M}{2} + 1, \dots, M. \end{cases} \quad (30)$$

$$\Delta f_{log} = \Delta f [\log(m+1) - \log(m)]; \quad m = 0, 1, \dots, M-1. \quad (31)$$

Figure 8 shows the CRBs comparison of stand and non-standard FDAs, which shows that these two non-standard FDAs also pose great difficulties in the FDOA reconnaissance methods but not TDOA's. This conclusion is consistent with the previous summary. Figure 9 shows the GDOP analysis of two non-standard FDA. Combine with Figure 4, GDOP differs significantly when the arrangement of Δf changed. Table 4 shows the RMSE comparison under standard and non-standard FDAs. CRB, GDOP and RMSE analysis all show that the arrangement of Δf has a very important impact on the performance of localization deception, which provides a theoretical basis for future array optimization design for

improved localization deception performance.

5 Conclusion

This paper analyzed the localization deception capability of FDA transmitted signals under passive bi-satellite reconnaissance. The time variation and periodicity of the FDA transmit beampattern caused by the frequency offset will reduce the accuracy of the FDOA. For TDOA, the FDA cannot cause too much difficulty in CRB theoretical analysis. From GDOP analysis, FDA has better localization deception performance when the emitter is closer to the subarray point. Theoretical analysis and simulation results show that the localization deception performance of FDA signals significantly outperforms PA signals in lower SNR conditions.

References

- 1 Youssef M, Mah M, Agrawal A K. Challenges: device-free passive localization for wireless environments. In: Proceedings of ACM/IEEE International Conference on Mobile Computing and Networking, 2007. 222–229
- 2 Olivadese D, Giusti E, Petri D, et al. Passive ISAR with DVB-T signals. *IEEE Trans Geosci Remote Sens*, 2013, 51: 4508–4517
- 3 Vaghefi R M, Gholami M R, Buehrer R M, et al. Cooperative received signal strength-based sensor localization with unknown transmit powers. *IEEE Trans Signal Process*, 2013, 61: 1389–1403
- 4 Hmam H. Passive source localization from time of arrival measurements. In: Proceedings of the 3rd International Symposium on Wireless Pervasive Computing, Santorini, 2008. 126–129
- 5 Li Y Y, Qi G Q, Sheng A D. General analytical formula of GDOP for TOA target localisation. *Electron Lett*, 2018, 54: 381–383
- 6 Jia T Y, Wang H Y, Shen X H, et al. Target localization based on structured total least squares with hybrid TDOA-AOA measurements. *Signal Process*, 2018, 143: 211–221
- 7 Qu X M, Xie L H. An efficient convex constrained weighted least squares source localization algorithm based on TDOA measurements. *Signal Process*, 2016, 119: 142–152
- 8 Yang S W, He Z S, Liu H M, et al. An analysis of anti-TDOA positioning capability for MIMO radar. In: Proceedings of International Workshop on Microwave and Millimeter Wave Circuits and System Technology, 2012
- 9 Gezici S, Tian Z, Giannakis G B, et al. Localization via ultra-wideband radios: a look at positioning aspects for future sensor networks. *IEEE Signal Process Mag*, 2005, 22: 70–84
- 10 Shi X R, Zhou F, Zhao B, et al. Deception jamming method based on micro-Doppler effect for vehicle target. *Sonar Nav*, 2016, 34: 1071–1079
- 11 Feng S, Wang G L, Ma W. Eliminating false localization from passive TDOA measurements. In: Proceedings of CIE International Conference on Radar, Guangzhou, 2016
- 12 Wang W Q. Adaptive RF stealth beamforming for frequency diverse array radar. In: Proceedings of the 23rd European Signal Processing Conference, 2015. 1163–1166
- 13 Fu Y J, Li Y, Huang Q D, et al. Design and analysis of LFM/Barker RF stealth signal waveform. In: Proceedings of Conference on Industrial Electronics and Applications, 2016. 591–595
- 14 Carson N, Martin S M, Starling J, et al. GPS spoofing detection and mitigation using cooperative adaptive cruise control system. In: Proceedings of IEEE Intelligent Vehicles Symposium (IV), Gothenburg, 2016. 1091–1096
- 15 Stein S. Algorithms for ambiguity function processing. *IEEE Trans Acoust Speech Signal Process*, 1981, 29: 588–599
- 16 Kim D G, Park G H, Kim H N, et al. Computationally efficient TDOA/FDOA estimation for unknown communication signals in electronic warfare systems. *IEEE Trans Aerosp Electron Syst*, 2018, 54: 77–89
- 17 Chen E Q, Tao R, Zhang W Q. Two-stage method for joint time delay and Doppler shift estimation. *IET Radar Sonar Nav*, 2008, 2: 71–77
- 18 Chestnut P C. Emitter location accuracy using TDOA and differential Doppler. *IEEE Trans Aerosp Electron Syst*, 1982, 18: 214–218
- 19 Torrieri D. Statistical theory of passive location systems. *IEEE Trans Aerosp Electron Syst*, 1984, 20: 183–198
- 20 Xu J W, Liao G S, Zhu S Q, et al. Deceptive jamming suppression with frequency diverse MIMO radar. *Signal Process*, 2015, 113: 9–17
- 21 Wang W Q, So H C, Farina A. An overview on time/frequency modulated array processing. *IEEE J Sel Top Signal Process*, 2017, 11: 228–246
- 22 Wen C, Tao M L, Peng J Y, et al. Clutter suppression for airborne FDA-MIMO radar using multi-waveform adaptive processing and auxiliary channel STAP. *Signal Process*, 2019, 154: 280–293
- 23 Wang W Q. Moving-target tracking by cognitive RF stealth radar using frequency diverse array antenna. *IEEE Trans Geosci Remote Sens*, 2016, 54: 3764–3773
- 24 Li Q, Huang L, So H C, et al. Beampattern synthesis for frequency diverse array via reweighted ℓ_1 iterative phase compensation. *IEEE Trans Aerosp Electron Syst*, 2018, 54: 467–475
- 25 Gui R, Wang W Q, Cui C, et al. Coherent pulsed-FDA radar receiver design with time-variance consideration: SINR and CRB analysis. *IEEE Trans Signal Process*, 2018, 66: 200–214
- 26 Khan W, Qureshi I M. Frequency diverse array radar with time-dependent frequency offset. *Antennas Wirel Propag Lett*, 2014, 13: 758–761
- 27 Han S D, Fan C Y, Huang X T. Frequency diverse array with time-dependent transmit weights. In: Proceedings of the 13th International Conference on Signal Processing, 2016. 448–451
- 28 Liu Y M, Ruan H, Wang L, et al. The random frequency diverse array: a new antenna structure for uncoupled direction-range indication in active sensing. *IEEE J Sel Top Signal Process*, 2017, 11: 295–308
- 29 Gao K D, Wang W Q, Cai J Y, et al. Decoupled frequency diverse array range-angle-dependent beampattern synthesis using non-linearly increasing frequency offsets. *IET Microw Antennas Propag*, 2016, 2014: 880–884
- 30 Xiong J, Wang W Q, Wang Z. Optimization of frequency increments via CRLB minimization for frequency diverse array. In: Proceedings of IEEE Radar Conference, Seattle, 2017. 0645–0650

- 31 Khan W, Qureshi I M, Saeed S. Frequency diverse array radar with logarithmically increasing frequency offset. *Antennas Wirel Propag Lett*, 2015, 14: 499–502
 32 Sengupta S K, Kay S M. Fundamentals of statistical signal processing: estimation theory. *Technometrics*, 1995, 37: 465
 33 Musicki D, Koch W. Geolocation using TDOA and FDOA measurements. In: *Proceedings of the 11th International Conference on Information Fusion*, Cologne, 2008

Appendix A

To prove (17), note that the elements of the Fisher information matrix $\mathbf{I}(\phi)$ for the complex Gaussian scenario PDF in (15) is a standard result given by [32]

$$\mathbf{I}(\phi)_{ij} = 2\text{Re} \left\{ \left[\frac{\partial \mathbf{s}(\phi)}{\partial \phi_i} \right]^H \mathbf{C}^{-1}(\phi) \left[\frac{\partial \mathbf{s}(\phi)}{\partial \phi_j} \right] \right\} + \text{tr} \left[\mathbf{C}_\phi^{-1} \frac{\partial \mathbf{C}_\phi}{\partial \phi_i} \mathbf{C}_\phi^{-1} \frac{\partial \mathbf{C}_\phi}{\partial \phi_j} \right], \quad (\text{A1})$$

$$\mathbf{C}(\phi) = \begin{bmatrix} \sigma_1 & 0 \\ 0 & \sigma_2 \end{bmatrix}. \quad (\text{A2})$$

The covariance matrices is not depend on interest parameters which means (A1) can be abbreviated as

$$\mathbf{I}(\phi)_{ij} = 2\text{Re} \left\{ \left[\frac{\partial \mathbf{s}(\phi)}{\partial \phi_i} \right]^H \mathbf{C}^{-1}(\phi) \left[\frac{\partial \mathbf{s}(\phi)}{\partial \phi_j} \right] \right\}, \quad (\text{A3})$$

formula $\frac{\partial \mathbf{s}(\phi)}{\partial \phi}$ can be considered by items. We get $\frac{\partial \mathbf{s}(\phi)}{\partial \tau}$ in (A4), where \mathbf{s}'_i , $i = 1, 2$ is the time-derivative of the received FDA signal by BPS. Similarly, we can also get $\frac{\partial \mathbf{s}(\phi)}{\partial f}$ shown in (A5).

$$\frac{\partial \mathbf{s}_\phi}{\partial \tau} = \begin{bmatrix} \frac{\partial \mathbf{s}_1}{\partial \tau} & \frac{\partial \mathbf{s}_2}{\partial \tau} \end{bmatrix}^T = \begin{bmatrix} \left(\frac{\partial \mathbf{s}_1}{\partial \tau_1} \right) & \left(\frac{\partial \mathbf{s}_2}{\partial \tau_2} \right) \\ \left(\frac{\partial \tau}{\partial \tau_1} \right) & \left(\frac{\partial \tau}{\partial \tau_2} \right) \end{bmatrix}^T = \begin{bmatrix} \frac{\partial \mathbf{s}_1}{\partial \tau_1} & -\frac{\partial \mathbf{s}_2}{\partial \tau_2} \end{bmatrix}^T = [-\mathbf{s}'_1 \ \mathbf{s}'_2]^T, \quad (\text{A4})$$

$$\frac{\partial \mathbf{s}_\phi}{\partial f} = \begin{bmatrix} \frac{\partial \mathbf{s}_1}{\partial f} & \frac{\partial \mathbf{s}_2}{\partial f} \end{bmatrix}^T = \begin{bmatrix} \left(\frac{\partial \mathbf{s}_1}{\partial \xi_1} \right) & \left(\frac{\partial \mathbf{s}_2}{\partial \xi_2} \right) \\ \left(\frac{\partial f}{\partial \xi_1} \right) & \left(\frac{\partial f}{\partial \xi_2} \right) \end{bmatrix}^T = \begin{bmatrix} \frac{\partial \mathbf{s}_1}{\partial \xi_1} & -\frac{\partial \mathbf{s}_2}{\partial \xi_2} \end{bmatrix}^T = [-\hat{\mathbf{s}}'_1 \ \hat{\mathbf{s}}'_2]^T, \quad (\text{A5})$$

where $\hat{\mathbf{s}}'_i$, $i = 1, 2$ is the frequency-derivative of the received FDA signal by BPS. After tedious calculations, Fisher information matrix $\mathbf{I}(\phi)$ is calculated as (A6). For the convenience of verification, discrete expressions are given here, and the continuous proof method is similar.

$$\mathbf{I}(\phi) = \begin{bmatrix} I_{11}(\phi) & I_{12}(\phi) \\ I_{21}(\phi) & I_{22}(\phi) \end{bmatrix}, \quad (\text{A6})$$

$$I_{11} = 2\text{Re} \left\{ \begin{bmatrix} -\mathbf{s}'_1 \\ \mathbf{s}'_2 \end{bmatrix}^H \mathbf{C}^{-1} \begin{bmatrix} -\mathbf{s}'_1 \\ \mathbf{s}'_2 \end{bmatrix} \right\} = \frac{2}{\sigma_1^2} \sum_{n=0}^{N-1} |\mathbf{s}'(\theta_i, r_i, nT_s - \tau_1)|^2 + \frac{2}{\sigma_2^2} \sum_{n=0}^{N-1} |\mathbf{s}'(\theta_i, r_i, nT_s - \tau_2)|^2, \quad (\text{A7})$$

$$I_{22} = 2\text{Re} \left\{ \begin{bmatrix} \hat{\mathbf{s}}'_1 \\ -\hat{\mathbf{s}}'_2 \end{bmatrix}^H \mathbf{C}^{-1} \begin{bmatrix} \hat{\mathbf{s}}'_1 \\ -\hat{\mathbf{s}}'_2 \end{bmatrix} \right\} = \frac{2T_s^2}{\sigma_1^2} \sum_{n=0}^{N-1} n^2 |\mathbf{s}(\theta_i, r_i, nT_s - \tau_1)|^2 + \frac{2T_s^2}{\sigma_2^2} \sum_{n=0}^{N-1} n^2 |\mathbf{s}(\theta_i, r_i, nT_s - \tau_2)|^2, \quad (\text{A8})$$

$$\begin{aligned} I_{12} = I_{21} &= 2\text{Re} \left\{ \begin{bmatrix} -\mathbf{s}'_1 \\ \mathbf{s}'_2 \end{bmatrix}^H \mathbf{C}^{-1} \begin{bmatrix} \hat{\mathbf{s}}'_1 \\ -\hat{\mathbf{s}}'_2 \end{bmatrix} \right\} = 2\text{Re} \left\{ -\mathbf{s}'_1{}^H \mathbf{C}_1^{-1} \mathbf{s}'_1 - \hat{\mathbf{s}}'_2{}^H \mathbf{C}_2^{-1} \hat{\mathbf{s}}'_2 \right\} \\ &= 2\text{Re} \left\{ \frac{1}{\sigma_1^2} \sum_{n=0}^{N-1} -jnT_s \mathbf{s}^*(\theta_i, r_i, nT_s - \tau_1) \mathbf{s}'(\theta_i, r_i, nT_s - \tau_1) \right\} \\ &\quad + 2\text{Re} \left\{ \frac{1}{\sigma_2^2} \sum_{n=0}^{N-1} -jnT_s \mathbf{s}^*(\theta_i, r_i, nT_s - \tau_2) \mathbf{s}'(\theta_i, r_i, nT_s - \tau_2) \right\}, \end{aligned} \quad (\text{A9})$$

$$\begin{aligned} \mathbf{s}(\theta_i, r_i, nT_s - \tau_i) &\approx \frac{1}{r_i} \exp[-j2\pi f_0(nT_s - \tau_i)] \\ &\quad \times \sum_{m=0}^{M-1} \exp \left\{ -j2\pi \left[\Delta f_m(nT_s - \tau_i) - \frac{f_0 m d \sin(\theta_i)}{c} - \frac{m \Delta f_m d \sin(\theta_i)}{c} \right] \right\}, \quad i = 1, 2, \end{aligned} \quad (\text{A10})$$

$$\begin{aligned} \mathbf{s}'(\theta_i, r_i, nT_s - \tau_i) &\approx \frac{j2\pi f_0}{r_i} \mathbf{s}(\theta_i, r_i, nT_s - \tau_i) + \frac{j2\pi}{r_i} \exp\{-j2\pi f_0(nT_s - \tau_i)\} \\ &\quad \times \sum_{m=0}^{M-1} \Delta f_m \exp \left\{ -j2\pi \left[\Delta f_m(nT_s - \tau_i) - \frac{f_0 m d \sin(\theta_i)}{c} - \frac{m \Delta f_m d \sin(\theta_i)}{c} \right] \right\}, \quad i = 1, 2. \end{aligned} \quad (\text{A11})$$